First estimates of the contribution of $CaCO_3$ precipitation to the release of CO_2 to the atmosphere during young sea ice growth

N.-X. Geilfus[1,2,3,*], G. Carnat[3], G.S. Dieckmann[4], N. Halden[3], G. Nehrke[4], T. Papakyriakou[3], J.-L. Tison[2] and B. Delille[1]

1. Unité d'Océanographie Chimique, Université de Liège, Allée du 6 aout, n°17, 4000 Liège, Belgium.

2. Laboratoire de Glaciologie, D.S.T.E, Université Libre de Bruxelles, Av. F. D. Roosevelt, 1050 Bruxelles, CP 160/03, Belgium.

3. now at University of Manitoba, Center of Earth Observation Science, 470 Wallace Bldg, 125 Dysart Road, Winnipeg, Canada.

4. Biogeosciences, Alfred Wegener Institute for Polar and Marine Research, Am Handelshafen 12, D-27570 Bremerhaven, Germany.

* Corresponding author: Nicolas-Xavier.Geilfus@ad.umanitoba.ca

Abstract

We report measurements of pH, total alkalinity, air-ice CO_2 fluxes (chamber method) and $CaCO_3$ content of frost flowers (FF) and thin landfast sea ice. As the temperature decreases, concentration of solutes in the brine skim (BS) increases. Along this gradual concentration process, some salts reach their solubility threshold and start precipitating. The precipitation of ikaite ($CaCO_3.6H_2O$) was confirmed in the FF and throughout the ice by Raman spectroscopy and X-ray analysis. The amount of ikaite precipitated was estimated to be 25 µmol kg^{-1} melted FF, in the FF and is shown to decrease from 19 µmol kg^{-1} to 15 µmol kg^{-1} melted ice in the upper part and at the bottom of the ice, respectively. CO_2 release due to precipitation of

$CaCO_3$ is estimated to be 50 μmol kg^{-1} melted samples. The dissolved inorganic carbon (DIC) normalized to a salinity of 10 exhibits significant depletion in the upper layer of the ice and in the FF. This DIC loss is estimated to be 2069 μmol kg^{-1} melted sample and corresponds to a CO_2 release from the ice to the atmosphere ranging from 20 to 40 mmol m^{-2} d^{-1}. This estimate is consistent with flux measurements of air-ice CO_2 exchange. Our measurements confirm previous laboratory findings that growing young sea ice acts as a source of CO_2 to the atmosphere. $CaCO_3$ precipitation during early ice growth appears to promote the release of CO_2 to the atmosphere however its contribution to the overall release by newly formed ice is most likely minor.

Keywords:

Chukchi Sea, sea ice, frost flowers, CO_2 fluxes, inorganic carbon, ikaite.

1. Introduction

Most carbon cycle research has not considered the possibility of either direct air-sea gas exchange in the presence of sea ice or indirect air-ice-ocean gas exchange, where sea ice play an active role in CO_2 transfer. Global and regional budgets of air-sea CO_2 exchange have ignored ice-covered regions [*Bates and Mathis*, 2009; *Takahashi et al.*, 2009], relying instead on the assumption that a sea ice cover is impermeable to gases. However, recent observations using both tower-based micrometeorological approaches and chamber sampling indicate that uptake and evasion of CO_2 does occur over sea ice [*Semiletov et al.*, 2004; *Delille*, 2006; *Zemmelink et al.*, 2006; *Semiletov et al.*, 2007; *Nomura et al.*, 2010b; *Nomura et al.*, 2010a; *Miller et al.*, 2011; *Papakyriakou and Miller*, 2011]. Observations of gas exchange have been attributed to numerous processes in sea ice, both physiochemical and biological, but the community is uncertain of the amount of CO_2 that sea ice can exchange with the atmosphere

and ocean, as well as the overall role played by sea ice as a sink or source of CO_2 to the atmosphere. In addition, current observations of gas exchanges vary by several orders of magnitude depending on the method. Fluxes reported by the chamber method [*Delille et al.*, 2007; *Nomura et al.*, 2010b; *Nomura et al.*, 2010a; *Geilfus et al.*, 2012] are significantly lower than fluxes measured by eddy covariance [*Semiletov et al.*, 2004; *Zemmelink et al.*, 2006; *Miller et al.*, 2011; *Papakyriakou and Miller*, 2011]. *Semiletov et al.* [2004] reported that melt ponds and open brine channels within sea ice represent a sink for atmospheric CO_2, of up to -39.3 mmol m^{-2} d^{-1}. *Papakyriakou and Miller* [2011] observed CO_2 fluxes over seasonal sea ice in the Canadian Arctic Archipelago to be highly variable, with hourly peak exchanges ranging from +86.4 mmol m^{-2} d^{-1} down to -259 mmol m^{-2} d^{-1}, during cold and warm phases (respectively) of the spring transition. The large but short-lived late-spring spike in sea ice uptake of atmospheric CO_2 corresponds in time to increased sea ice permeability and a corresponding rapid increase in brine volume associated with opening of brine channels, leading the authors to speculate that the downward flux was driven in part by photosynthesis at the ice base. Using the chamber method, *Delille* [2006] measured CO_2 fluxes, ranging from -4 mmol m^{-2} d^{-1} to +2 mmol m^{-2} d^{-1} over Antarctic pack ice, and related these fluxes to the seasonal differences in brine pCO_2 relative to the atmospheric concentration. *Nomura et al.* [2010b] also measured CO_2 fluxes ranging from -1 mmol m^{-2} d^{-1} to +0.7 mmol m^{-2} d^{-1} using chambers over warming first year land-fast sea ice in Barrow in the late spring. *Delille* [2006] and *Nomura et al.* [2010b] ascribed the flux direction to the difference in air-sea ice brine pCO_2.

The studies outlined above document fluxes over mature, slow - growing or decaying seasonal sea ice. Fluxes over growing artificial sea ice have been reported by *Nomura et al.* [2006], however comparative field measurements of fluxes over thin, rapidly growing sea ice

do not exist. This represents a significant gap in our understanding of CO_2 exchange over the annual growth/decay sea ice cycle.

As mentioned, uncertainty remains regarding the exact drivers of the CO_2 exchange across the air - sea ice - ocean interface, although several potential processes have been identified. As sea ice forms and grows thicker, salts are partly rejected from the sea ice and partly trapped within the sea ice structure, concentrated into brine pockets, tubes and channels in the sea ice [*Weeks and Ackley*, 1982]. A reduction in the brine temperature promotes increased brine salinity and concentration of solutes (including DIC), and increased brine pCO_2 through a decrease in brine CO_2 solubility [*Papadimitriou et al.*, 2004]. Significant changes in the mineral-liquid thermodynamic equilibrium can occur with changes in temperature, leading to sequential mineral precipitation [*Marion*, 2001]. Ikaite, a hexahydrate polymorph of calcium carbonate ($CaCO_3.6H_2O$), begins to precipitate at -2.2°C, mirabilite ($Na_2SO_4.\ 10H_2O$) below -8°C. $NaCl.2H_2O$ precipitates below -26°C, while potassium and magnesium salts precipitate below -34°C [*Assur*, 1958; *Rankin et al.*, 2000; *Marion*, 2001]. The precipitation of calcium carbonate from the brine [*Papadimitriou et al.*, 2004; 2008; *Dieckmann et al.*, 2010] also increases the brine pCO_2. Sea ice hosts a complex biological system [*Thomas et al.*, 2010] and carbon is cycled through the processes of photosynthesis and respiration associated with seasonally large algal communities [*Arrigo et al.*, 2010] and bacterial communities that are thought to function throughout the annual cycle [*Deming*, 2010]. CO_2 can be exchanged among sea ice brine, seawater and atmosphere, as long as the ice remains permeable [*Nomura et al.*, 2006; *Rysgaard et al.*, 2007; *Loose et al.*, 2009].

The possible role of $CaCO_3$ precipitation on sea ice carbonate biochemistry has received growing attention. *Rysgaard et al.* [2007; 2009] suggested that calcium carbonate precipitation in sea ice could act as a significant sink for atmospheric CO_2. An abiotic pump would result from the high DIC: TA ratio (TA being defined as the total alkalinity) of brine

95 expelled from sea ice during the ice growth and brine drainage as a consequence of $CaCO_3$
96 precipitation, which is described by:

97 $$2HCO_3^- + Ca^{2+} \leftrightarrow CaCO_3 + H_2O + CO_2 \quad (1)$$

98 Precipitation of 1 mole of $CaCO_3$ transfers HCO_3^- to the CO_2 pool, decreasing DIC by 1 mole
99 and TA by 2 moles. According to *Rysgaard et al.* [2007], this pump could represent a
100 downward transport of 0.2 - 0.5 Pg C y^{-1} out of the surface ocean. However the role and
101 significance of $CaCO_3$ formation/dissolution in sea ice on atmospheric CO_2 depends on the
102 rate of mineral production and sea ice permeability; the latter depending on the conditions and
103 timing of precipitation and the fate of the precipitate [*Delille*, 2006].

104 The authigenesis of ikaite in natural sea ice is not yet fully understood. Little is known about
105 the spatial and temporal occurrence of ikaite precipitates in sea ice, but recent discovery of
106 ikaite in sea ice at both poles indicates that ikaite precipitation is not a localized phenomenon
107 [*Dieckmann et al.*, 2008; 2010]. Ikaite stability is limited to near-freezing temperatures and is
108 apparently favored by alkaline conditions, elevated phosphate concentrations and by the
109 presence of certain additives like amino acids [*J L Bischoff et al.*, 1993a; *Whiticar and Suess*,
110 1998; *Buchardt et al.*, 2001; *Selleck et al.*, 2007].

111 In addition to the abiotic pump suggested by *Rysgaard et al.,* [2007; 2009], $CaCO_3$
112 precipitation at the top of sea ice is thought to play a role in atmospheric chemistry as a
113 trigger for the transformation of inert sea-salt bromide to reactive bromine monoxide and the
114 occurrence of tropospheric ozone depletion events (ODEs) at high latitudes [*Sander et al.*,
115 2006]. It was suggested that this conversion was possibly due to an alkalinity decrease
116 [*Sander et al.*, 2006]. However, *Morin et al.* [2008] pointed out that the alkalinity decrease
117 required for such transformation may not occur in sea ice and that further work is needed to
118 resolve this issue. *Piot et al.* [2008] showed that the precipitation of calcium carbonate

119 ($CaCO_3$) in sea ice brine is a key process allowing for the rapid acidification of aerosols
120 originating from frost flowers (FF), highlighting the potential importance of FF for ozone
121 chemistry in the Arctic. Their work supports earlier suggestions that FF and their
122 accompanying brine skim (BS) may play an important role as a source of salt aerosols for the
123 atmosphere [*Rankin et al.*, 2000; 2002; *Alvarez-Aviles et al.*, 2008]. FF mainly grow on newly
124 formed sea ice [*Perovich and Richter-Menge*, 1994; *Alvarez-Aviles et al.*, 2008], and are
125 centimeter-scale ice structures, formed by a mixture of atmospheric hoar and liquid from the
126 BS, brine expelled from the ice crystals during the sea ice growth. The latter explains the
127 observed high bulk salinity of FF. Growth is thought to proceed in three stages [*Alvarez-*
128 *Aviles et al.*, 2008]: (i) development of small nodules on nilas, (ii) the initial formation of FF
129 on the nodules, and (iii) their subsequent growth into mature structures.

130 To the best of our knowledge, field measurements of CO_2-related parameters have not yet
131 been reported over young, rapidly forming sea ice; laboratory experiments suggest than young
132 newly formed sea ice releases CO_2 to the atmosphere [*Nomura et al.*, 2006]. During fieldwork
133 in Barrow (Alaska) in 2009, we had the opportunity to sample a newly formed ice sheet and
134 associated FF. In this paper quantitative analysis of pH, TA and amount of ikaite precipitates
135 in FF and bulk sea ice identified the influence of an abiotic process on the sea ice carbonate
136 system during the early growth phase and to demonstrate calcium carbonate precipitation as
137 ikaite. Furthermore, we report the first Arctic measurements of air-sea CO_2 fluxes over young
138 growing ice and FF and provide a first assessment of the contribution of $CaCO_3$ precipitation
139 to the total observed CO_2 release to the atmosphere from those media.

140 2. Methods

141 Individual FF, surface BS and young sea ice cores (20 cm thick) were collected from young
142 shore-fast sea ice near Barrow, Alaska, on April 6, 2009 (Fig. 1). A half dozen FF were

143 sampled by scrapping the ice surface using a clean spatula and were stored frozen in a clean
144 plastic bag. A Teflon coated stainless steel ice corer with an internal diameter of 7 cm was
145 used to sample a total of 5 cores from the young ice in an area of 1 m² with a maximum
146 spacing between cores of 20 cm. Sea ice temperature was measured *in-situ* directly after
147 extraction of the first core, using a calibrated probe (TESTO 720) inserted in pre-drilled holes
148 (perpendicular to the vertical in the side of the core) at the exact diameter of the probe and
149 with a depth resolution of 2.5 cm in the vertical with ±0.1°C precision (not including potential
150 bias from the heat transfer during drilling or temperature change during temperature
151 measurements). Sea ice cores and FF samples were stored on the sampling site in an isolated
152 box filled with individual cooling bags, pre-cooled at -30°C. Back in the lab, samples were
153 kept frozen at -28°C. In the lab, the temperature core was cut into successive 2.5 cm thick
154 slices. Each slice was stored in a bucket and left to melt at +4°C in the dark. Salinity of the
155 melt water was measured with a Thermo-Orion® portable salinometer WP-84TPS meter with
156 a precision of ±0.1. The brine volume fraction was calculated using the equations given by
157 *Eicken* [2003] and references therein.

158 Vertical thin sections were performed on one of the cores following standard procedures
159 [*Tison et al.*, 2008], in order to describe the texture of the ice. Pictures of crystal texture were
160 taken of the thin sections using a light table and cross- and parallel- polarized sheets with a
161 macro setting on a camera (Nikon® Coolpix S200, 7.1 mega-pixels).

162 Another core was cut into vertical sections at a 5 cm depth resolution. From each section, 20 g
163 of ice was melted at room temperature to measure phosphate using standard colorimetric
164 procedure on a Genesys® spectrophotometer [*Grasshoff et al.*, 1983].

165 Fluxes of CO_2 at the sea ice – atmosphere interface were measured using an accumulation
166 chamber (West System®) at four places over the sampling site in an area of $2m^2$. The

chamber is a metal cylinder closed at the top, with an internal diameter of 20 cm and an internal height of 9.7 cm. A rubber seal surrounded by a serrated metal edge ensured an airtight connection between the ice and the accumulation chamber. The chamber was connected in a closed loop to an infrared gas analyzer (Licor® 6262) using an air pump set at 3 L min^{-1}. The measurement of pCO_2 in the chamber was recorded every 30 sec for a minimum of 5 min. The flux was then computed from the slope of the linear regression of pCO_2 against time ($r^2>0.99$) according to *Frankignoulle* [1988]. Uncertainty of the flux computation due to the standard error on the regression slope was ±3% on average.

Crystals of calcium carbonate were extracted from the ice cores following *Dieckmann et al.* [2008]. Ice cores were cut into 5 cm sections, which were then transferred into clean plastic containers, sealed and melted at +4°C. Samples were processed as soon as they were melted. Melt water temperature never rose significantly above 0°C. The melt water was gently swirled so most of the crystals settled in the central part of the container. Using the first ice core, a proportion of the crystals were collected for direct observation under a binocular microscope, while the rest of the crystals were stored on 0.2 µm Millipore filters which were rinsed with 75% ethanol and kept frozen at -25°C for later identification of the mineralogical phase. On a twin ice core, the same melting process was followed but the crystals were pipetted into a glass vial containing 60% ethanol and kept frozen at -18°C for the identification of the mineralogical phase.

Crystals identification were carried out by X-ray diffraction using a Siemens® (Bruker) D5000 Powder Diffractometer at room temperature. Bruker's DIFFRACplus software and MDI Jade + software were used to collect and analyze the data. The goniometer was configured in Bragg-Brentano (θ-2θ) geometry and used Cu radiation (Cu Kα1 λ = 1.54060). The system was equipped with computer-controlled divergence and receiving slits, a rotating sample holder, diffracted beam graphite monochromator and a scintillation detector. Scanning

192 electron microscopy (SEM) was performed on a single crystal, from the same filter used for
193 the X-ray (left one day at room temperature). The instrument used was a Cambridge®
194 Stereoscan 120, running at 20 keV. Others analyses using a confocal Raman microscope
195 (WITec®, Ulm, Germany) were performed for phase identification of the crystals extracted.
196 The Raman was equipped with a diode laser (532 nm) and an Olympus® 20x Teflon coated
197 water objective. The sample was transferred in a temperature-controlled room into cooled (~
198 1°C) glass Petri dishes and transferred to the Raman microscope. The ikaite stayed stable for
199 at least 15 minutes with this approach, before signs of transformation into calcite were
200 observed. Time was sufficient for reliable phase identification of ikaite given that the
201 measurement took only a few seconds.

202 The size of $CaCO_3$ crystals found in our sample ranged from <40 µm to 200 µm (Fig. 2), so
203 they could all be removed by filtration on 0.2 µm filters. According to previous work of
204 *Rysgaard et al.* [2007] and [2009], we assumed that dissolution of $CaCO_3$ crystals during the
205 melting process was not significant, and attention was paid to keep the sample below +4°C at
206 all time during melting process, filtration and pH measurement. The overall calcium
207 carbonate content ($\Delta CaCO_3$) was then estimated from the difference between the alkalinity of
208 unfiltered sample, denoted as bulk alkalinity (TA_b) and the sample filtered on 0.2 µm
209 Millipore filters, denoted as filtered alkalinity (TA_f). $\Delta CaCO_3$ is computed according to:

210 $$\Delta CaCO_3 = \frac{1}{2}\,(TA_b - TA_f) \qquad (2)$$

211 Ice cores and FF were then melted and processed according to the following methodology in
212 order to estimate the amount of precipitated $CaCO_3$. Twin ice cores, cut into 5 cm segments
213 and FF were transferred into Tedlar® gas sampling bags, closed with a 30 cm gas-tight Tygon
214 tube. The excess air was quickly removed through the valve. The ice samples were melted in
215 a fridge at +4°C. As soon as the ice was completely melted, samples were collected to

measure pH, TA_b and TA_f. The melt water was shaken, re-suspending the crystals and leaving the liquid homogenized. First, samples for TA_b were collected, then samples for TA_f. The filtration was carried out at +4°C to avoid any calcium carbonate dissolution. Then, pH was measured using a Metrohm® combined electrode calibrated at temperatures ranging from +1°C to +4°C on the total hydrogen ion scale using TRIS (2-amino-2hydroxymethyl-1.3-propanediol) and AMP (2-aminopyridine) buffers prepared at salinities of 35 and 75 according to the formulations proposed by *DOE* [1994]. The pH measurements were carried out at below +4°C. The accuracy of pH measurements was ±0.01 pH units [*Frankignoulle and Borges*, 2001]. TA was measured by open-cell titration with HCl 0.1 M according to *Gran* [1952] on 50 ml of sea ice melt water samples. Titration was stopped for 10 minutes at pH 4.2 to ensure that all $CaCO_3$ crystals were dissolved prior to TA measurement over the pH range 3 and 4.2 as required for the Gran function. The accuracy of TA measurements was ± 4 µmol kg^{-1}. Data were quality checked with certified reference material acquired from Andrew Dickson (Scripps Institution of Oceanography, University of California, San Diego). DIC_b and DIC_f were computed from pH and TA_b and TA_f, respectively according to CO_2 acidity constants of *Mehrbach et al.* [1973] refitted by *Dickson and Millero* [1987] and other constants advocated by *DOE* [1994]. We assumed a conservative behavior of CO_2 dissociation constants at subzero temperatures because *Delille et al.* [2007] and *Marion et al.* [2001] suggested that thermodynamic constants relevant for the carbonate system can be assumed to be valid at subzero temperatures. DIC_f is not influenced by calcium carbonate dissolution after sampling. DIC_b obtained from TA_b was used for the sake of consistency with the previous work of *Rysgaard et al.* [2007] and [2009].

The age of the ice was roughly estimated using the air and sea temperature records from the location of the Barrow Sea Ice Mass Balance Buoy (data available at http://seaice.alaska.edu/gi/data) at the time of the sampling [*Druckenmiller et al.*, 2009]. The

time since formation, Δt, was estimated by subtracting the change in the ice thickness, H_i, for each time step until $H_i = 0$ [*Lepparanta*, 1993] according to:

$$\Delta H_i = \frac{K_i}{H_i \rho_b L}(T_w - T_a)\Delta t \quad (3)$$

where ρ_b is the sea ice bulk density, K_i the thermal conductivity of the ice and T_w and T_a the seawater and air temperatures, respectively. The thermal conductivity and the sea ice bulk density were calculated using the formulation as suggested by *Eicken* [2003] and references therein. The latent heat of fusion, L, was kept at 333.9 kJ kg^{-1}. We assumed that T_a and T_w observed at the mass balance site was representative for larger area and that oceanic heat flux was negligible.

3. Results

3.1. Sea ice properties

The young sea ice was about 20 cm thick (±1 cm). A strong temperature gradient was observed between the atmosphere (T = -23°C), the FF (T = -19°C) and the sea ice interface with the atmosphere (T = -14.2°C). The salinity profile was C-shaped, with a salinity of 31.5 at the top of the ice and 11.2 at the bottom (Fig. 3), which is typical for new Arctic sea ice [*Ehn et al.*, 2007]. According to *Golden et al.* [2007], a permeability threshold occurs for a brine volume of 5%. Therefore, this young sea ice was permeable throughout the whole thickness allowing exchanges of matter with the atmosphere or the water column.

A high salinity BS (S = 114) covered the ice surface and FF were observed (Fig. 4). BS is the result of the upward expulsion of brine associated with sea ice crystal growth, and is facilitated by the high porosity within a few centimeters of the surface layer [*Perovich and Richter-Menge*, 1994]. The upper part of the sea ice column was characterized by a distinct

263 layer of fine-grained granular ice (FG) directly followed by a layer of granular ice (G, Fig. 4).
264 At 4 cm depth, there was a 2 cm zone of transition between the granular ice and columnar ice
265 (G/C). The rest of the sea ice cover was formed of columnar ice, except at 8 cm depth where a
266 very thin layer (few mm) of granular ice was present.

267 Using T_a and T_w at the mass balance site, equation (3) suggests that sea ice reached the
268 thickness observed at the time of sampling after only 45.5 hours. However, the ice was
269 estimated to be 1 week by a local "interpreter" that is consistent with the observed level of
270 frost flower degradation [*Bowman and Deming*, 2010].

271 ### *3.2. Carbonate system*

272 The pH ranged from 8.7 to 9.5 in the upper layer of young sea ice while FF exhibited a pH of
273 9.0 (Fig. 5a). The pH measured in FF or young sea ice was of the same order of magnitude as
274 observed previously [*Gleitz et al.*, 1995; *Delille et al.*, 2007; *Papadimitriou et al.*, 2007]. TA_f
275 and DIC_f concentration in sea ice ranged from 492 µmol kg^{-1} melted sea ice to 863 µmol kg^{-1}
276 melted sea ice and from 418 µmol kg^{-1} to 488 µmol kg^{-1} melted sea ice, respectively, while
277 TA_f and DIC_f were much higher in FF (2586 µmol kg^{-1} melted FF and 1183 µmol kg^{-1} melted
278 FF, respectively) (Fig. 5b). These results were of the same order of magnitude as the
279 observations of *Rysgaard et al.* [2007] and [2009] for Arctic sea ice.
280 DIC_f normalized to a salinity of 10 (DIC_{10}, 10 is the mean salinity of this young sea ice),
281 allows us to elucidate variations in DIC_f (Fig. 5c) independent of salinity changes. FF and the
282 upper layer of the young sea ice showed a strong decrease in DIC_{10} value while the rest of the
283 ice column was relatively homogeneous (around 520 µmol kg^{-1} melted sea ice).
284 The TA_b: DIC_b ratio in our young sea ice samples ranged from 1.12 to 1.79 in the upper layers
285 with a value peaking at 2.05 in the FF (Fig. 5e). According to *Rysgaard et al.* [2007] and
286 [2009], a ratio TA_b: DIC_b as high as 2 indicates that calcium carbonate precipitation occurred.

This precipitation has been estimated by the difference between the TA_b and TA_f, following the equation (2) to be about 25 µmol kg^{-1} melted FF in the FF, decreasing from 19.4 µmol kg^{-1} melted sea ice in the upper part of the ice to 15 µmol kg^{-1} melted sea ice in the bottom of the ice (Fig. 5f). These estimates might be underestimates, as the method does not account for potential $CaCO_3$ dissolution during melting of the ice prior to sub-sampling for TA.

3.3. Air-ice CO_2 fluxes

Four measurements of CO_2 fluxes were taken at the sea ice interface with the atmosphere. The fluxes ranged from 4.2 mmol m^{-2} d^{-1} to 9.9 mmol m^{-2} d^{-1} (positive flux denoting gas evasion), with an overall mean of 6.7 mmol m^{-2} d^{-1}, the magnitudes of which compare reasonably well with values previously reported over sea ice in spring and summer by *Delille* [2006] and *Nomura et al.* [2010a] using the chamber method. However, the fluxes were opposite in direction as, according to *Nomura et al.* [2006], the initial sea ice growth was expected to release CO_2 to the atmosphere.

3.4. Precipitation of minerals

Various analyses were carried out on crystals found in samples of sea ice melted at +4°C. Crystals were found at all depths sampled in young sea ice and in FF. First observations under a binocular microscope at room temperature revealed that crystals ranged from <40 µm to 200 µm (Fig. 2b). Their morphology was relatively similar to that of the crystals found by *Dieckmann et al.* [2008] but they were significantly smaller. After a few minutes under the binocular, their appearance became milky, a phenomenon also observed by *Whiticar and Suess* [1998] and *Dieckmann et al.* [2010]. This could be due to the transformation of ikaite ($CaCO_3.6H_2O$) into calcite, $CaCO_3$, with increasing crystal temperatures. No clear X-ray diffraction pattern could be obtained from crystals stored on Millipore filters (Fig. 6a, b, c) even if they had perfect crystal faces. Again, the change of phase as a result of warming

311 during X-ray scanning of the sample may have been responsible for these unidentifiable X-ray
312 patterns. A clear X-ray pattern was finally obtained after leaving the crystals for 1 day at room
313 temperature (Fig. 6d); calcite and halite were the two minerals identified by the X-ray scan in
314 this case, as illustrated by the patterns of calcite and halite shown in figure 6e and 6d. A SEM
315 performed on the same crystals confirmed the presence of calcite, with 84% of the total
316 weight of these crystals in Ca. The Raman spectra of the precipitate and two reference
317 samples (natural calcite and freshly precipitated ikaite) are given in figure 7. The spectra
318 showed the typical internal vibration modes of the symmetric stretch of the carbonate ion v_1
319 (1085 cm^{-1} calcite and 1075 cm^{-1} for ikaite) and its in-plane band v_4 (715 cm^{-1} calcite and 723
320 cm^{-1} ikaite) [*W D Bischoff et al.*, 1985] and the lattice modes in the range between 100 cm^{-1}
321 and 300 cm^{-1} were visible. The three duplets at ~150, 200, and 270 cm^{-1} in the ikaite spectra
322 strongly depend on its crystallographic orientation. However, the large difference in the peak
323 positions of the internal modes v_1 and v_4 of calcite and ikaite made it possible to
324 unambiguously distinguish between these two phases. Raman spectra determined on a set of
325 different samples showed ikaite to be the only mineral phase present. These measurements
326 were performed systematically every 5 cm throughout the ice core.

327 4. Discussion

328 As sea ice grows, brine expulsion promotes a buildup of a high salinity layer on top of the ice,
329 the BS, allowing several processes to take place. Firstly, it leads to FF formation [*Perovich*
330 *and Richter-Menge*, 1994; *Alvarez-Aviles et al.*, 2008] and favors direct exchanges with the
331 atmosphere [*Alvarez-Aviles et al.*, 2008; *Bowman and Deming*, 2010]. Secondly, as the BS
332 concentration increases with the decreasing temperatures, some salts may reach their
333 solubility threshold and start precipitating. Recent studies based on field observations [*Delille*,
334 2006; *Delille et al.*, 2007; *Papadimitriou et al.*, 2007; *Dieckmann et al.*, 2008; *Rysgaard et*

335 *al.*, 2009; *Munro et al.*, 2010] and on laboratory freezing experiments [*Papadimitriou et al.*,
336 2004; *Nomura et al.*, 2006] indicate that precipitation of $CaCO_3$ occurs within sea ice. The
337 precipitation of ikaite was found in FF and throughout the sea ice but was not uniformly
338 distributed with depth in the ice cores. Estimations of the amount precipitated, through the
339 TA_b - TA_f difference, showed a C-shape with maxima in the FF (25 µmol kg^{-1} melted FF) and
340 at the bottom (15 µmol kg^{-1} melted sea ice, Fig. 5). This shape could be due to the expulsion
341 of salty supersaturated brine from the sea ice to the atmosphere and to the underlying
342 seawater. The TA_b: DIC_b ratio also showed a maximum in the FF. According to *Rysgaard et*
343 *al.* [2007] and [*2009*], a ratio TA_b: DIC_b as high as 2 indicates the precipitation of calcium
344 carbonate. Our results point out that this precipitation occurs with a lower TA_b: DIC_b ratio and
345 seems to be favored at the surface due to the expulsion of salty supersaturated brine.
346 Ikaite precipitation in a natural sea ice environment requires several conditions. The saturation
347 state of ikaite is below the saturation at all temperatures in seawater but it rapidly approaches
348 saturation near 0°C. Nevertheless, ikaite cannot form directly by the cooling of seawater [*J L*
349 *Bischoff et al.*, 1993a]. The solution from which it forms must, at least temporarily, be
350 supersaturated with respect to ikaite. This supersaturation is most likely to occur near 0°C but
351 even then, external additions of either Ca^{2+} or HCO_3^- are required [*J L Bischoff et al.*, 1993a].
352 Furthermore, natural occurrence of ikaite requires conditions which also inhibit the
353 precipitation of more stable anhydrous forms of $CaCO_3$ [*J L Bischoff et al.*, 1993a].
354 Orthophosphate prevents the crystallization of the more stable anhydrous forms of $CaCO_3$,
355 even at concentrations as low as 5 µM, but does not interact with ikaite [*J L Bischoff et al.*,
356 1993a; *Buchardt et al.*, 2001]. Accordingly, high PO_4^{3-} concentration have been linked to
357 ikaite precipitation in Antarctic and Arctic sediments [*Kennedy et al.*, 1987; *Whiticar and*
358 *Suess*, 1998] and other various environments [*J L Bischoff et al.*, 1993b; *Buchardt*, 2004;
359 *Selleck et al.*, 2007]. Hence, ikaite precipitation seems to be favored by near-freezing

360 temperatures, alkaline conditions, elevated phosphate concentrations [*J L Bischoff et al.*,
361 1993a; *Buchardt et al.*, 2001; *Selleck et al.*, 2007] and/or by the presence of certain additives
362 like amino acids [*Whiticar and Suess*, 1998].

363 With a surface temperature ranging from -9.9°C to -14°C, temperature was not a limiting
364 factor to calcium carbonate precipitation. The phosphate concentration in the ice column
365 ranged from 0.38 µM to 0.7 µM while the FF concentration was 2.45 µM. These
366 concentrations are comparable with previous studies of Arctic sea ice [*Krembs et al.*, 2002;
367 *Lee et al.*, 2008; *Mathis et al.*, 2009] except for the FF where the PO_4^{3-} concentration is
368 significantly higher. The alkalinity condition was also satisfied at this station with a pH of 9
369 in the FF. According to *Whiticar et al.* [1998], the presence of amino acids and phosphates at
370 cold temperatures allows ikaite to form preferentially over calcite or aragonite but this feature
371 is not a universal requirement. *Bowman et al.* [2010] collected samples with us (i.e. same day,
372 same sampling site) and measured high concentrations of particulate exopolymeric substances
373 (pEPS) up to 36.5 mg gluceq ml^{-1}, 725 mg gluceq ml^{-1} and 1420 mg gluceq ml^{-1} in melted sea
374 ice, BS and melted FF, respectively. They pointed out the role of bacterial activity in
375 providing ice-nucleating particles through pEPS production. As suggested by [*Whiticar and*
376 *Suess*, 1998] pEPS could also act as calcium carbonate precipitation nuclei; high pEPS
377 production measured in Barrow likely promoted ikaite formation. On the whole, lower
378 temperatures and higher phosphate and pEPS concentration were observed in the BS and FF
379 compared to sea ice, promoting ikaite formation in the surface layers.

380 Our observations of TA and pH in the top layer of ice in Barrow challenges previous
381 hypothesis by *Sanders et al.* [2006] that significant precipitation of $CaCO_3$ in sea ice and FF
382 significantly reduces the pH buffering capacity of sea ice allowing for a significant decrease
383 in pH. To our best knowledge, pH in sea ice ranges from 7.78 to 9.89 [*Gleitz et al.*, 1995;

384 *Delille et al.*, 2007; *Papadimitriou et al.*, 2007] with a rather elevated higher end value and a
385 much larger range than proposed by *Sander et al.* [2006] (reported range: 2 to 8).

386 In both artificial and natural sea ice, a depletion in DIC was observed in sea ice brine
387 [*Papadimitriou et al.*, 2004] and in the ice [*Munro et al.*, 2010] that could not be ascribed to
388 biological activity. In both cases, the authors suggest that $CaCO_3$ precipitation and CO_2
389 degassing may occur in sea ice without being able to elucidate the processes by which these
390 phenomena occur. We observed a strong decrease of the DIC_{10} in the upper layer of the ice
391 column and in the FF. We attempt to assess the overall depletion in the upper layer by
392 assuming that DIC_{10} should be homogeneous over the ice column as should be the case if no
393 biogeochemical processes occur (*i.e.* primary production, $CaCO_3$ precipitation and CO_2
394 transfer to the gas phase). We then take into account DIC_f at 7.5 cm ($DIC_{7.5cm}$ and compute
395 DIC_{th} as the value of $DIC_{7.5cm}$ extrapolated to the salinity encountered in the upper part of the
396 ice column assuming a linear relationship between DIC and salinity). DIC_{th} at a given depth i
397 was then computed according to:

398 $$DIC_{th} = \frac{DIC_{7.5\ cm} * S_i}{S_{7.5\ cm}} \quad (5)$$

399 Where $DIC_{7.5cm}$ is the DIC at 7.5 cm, $S_{7.5cm}$ and S_i are the salinities at 7.5 cm and at a given
400 depth *i*, respectively. The difference between the DIC_f (Fig. 5d) and the DIC_{th} represents the
401 loss of DIC, illustrated by the hatched area in Fig. 5d. This loss is estimated to be 2069 µmol
402 kg^{-1} melted sample, from the FF down to 7.5cm depth. Only a few studies estimate the
403 primary production in Arctic sea ice and the results range widely, from 0.03 mg C m^{-2} d^{-1} to
404 463 mg C m^{-2} d^{-1} [*Arrigo et al.*, 2010]. *Gosselin et al.* [1997] reported a rate of production of
405 47 mg C m^{-2} d^{-1} in an area between 70 – 75°N and 169 – 170°W during Arctic summer.
406 Considering an ice thickness of 1 m, this production is about 19.6 µmol C kg^{-1} d^{-1}. Applying
407 this rate to an ice cover of 20 cm during 7 days, we found a production of 19.6 µmol C kg^{-1} d^{-}

408 [1]. Integrated for 7 days, this yields production of 137 μmol C kg^{-1}, which corresponds to only
409 6.7 % of the DIC depletion observed. This is probably an overestimate as *Arrigo and Sullivan*
410 [1992] found greatly reduced photosynthetic rates in fast ice at brine salinities higher than 50
411 and total photosynthetic shutdown at brine salinity higher than 100, which is the range of
412 salinity found at this station within the upper 10 cm of ice. According to the amount of
413 calcium carbonate precipitated in the FF (25 μmol kg^{-1} melted FF) and in the top 10 cm of the
414 ice (19 + 6 μmol kg^{-1} melted sea ice), the CO_2 generated by this precipitation corresponds
415 only to 50 μmol kg^{-1} of melted sample. The part of the precipitation process in the release of
416 CO_2 from the BS and/or FF is therefore minor compared to the total exchanges of 2069 μmol
417 kg^{-1} melted sample estimated from the DIC depletion. In the same way *Munro et al.* [2010]
418 used $\delta^{13}C_{DIC}$ to determine the fractional contributions of $CaCO_3$ precipitation and CO_2
419 degassing. They found that degassing seems to be solely responsible for DIC depletion.
420 Therefore we consider that the contribution of primary production and calcium carbonate
421 precipitation to DIC depletion are negligible, at least near the top of the ice. DIC depletion
422 then mainly corresponds to a release of CO_2 from the ice to the atmosphere during the upward
423 expulsion of brine supersaturated in CO_2. According to several studies [*Rankin et al.*, 2000;
424 2002; *Alvarez-Aviles et al.*, 2008; *Bowman and Deming*, 2010], FF and BS facilitate salt
425 transport (or other materials) to the atmosphere and frost flowers increase the specific surface
426 area of the ice of about 40% [*Domine et al.*, 2005]. Also, enhanced salt transport, related brine
427 concentration, and increase of specific surface area potentially promote CO_2 degassing.

428 Our results indicate that DIC loss in the top 7.5 cm of the ice was 2069 μmol kg^{-1} melted
429 sample. Considering a mean sea ice density of 910 kg m^{-3} [*Timco and Frederking*, 1996], the
430 mass of the top 7.5 cm of ice in direct interaction with the atmosphere is estimated to be 68 kg
431 per square meter of ice. Therefore, 1 m^2 of ice loses about 141.2 mmol $kg^{-1}$of DIC. If the ice
432 is between 2 and 7 days old, this loss of DIC would correspond to a CO_2 flux ranging from 20

433 to 40 mmol m^{-2} d^{-1}. This efflux is approximately 4 times larger than CO_2 flux measured with
434 the chamber method during our relatively short sampling period, which ranged from 4.2 mmol
435 m^{-2} d^{-1} to 9.9 mmol m^{-2} d^{-1}. Air-ice CO_2 fluxes are modulated by ice permeability (linked to
436 sea ice porosity), but also snow permeability and air-ice pCO_2 gradients. These parameters are
437 likely to evolve rapidly during sea ice growth, together with temperature and bulk salinity for
438 permeability [*Golden et al.*, 2007], and brine concentration and air-ice CO_2 exchanges
439 [*Delille*, 2006; *Delille et al.*, 2007; *Nomura et al.*, 2010b; *Geilfus et al.*, 2012] for air-ice pCO_2
440 gradients. The CO_2 fluxes measurements provided by the chamber method only provide a
441 snapshot that does not account for past processes, while the CO_2 deficit method accounts for
442 the overall CO_2 release of the past days, probably right from the beginning of the ice
443 formation. The deficit method presented above is therefore a more robust method than
444 chamber measurements in providing a budget of air-ice CO_2 fluxes integrated over the time.

445 # 5. Conclusions

446 Raman and X-ray analysis of thin shore fast ice and FF collected in Barrow, Alaska, show
447 conspicuous evidence of calcium carbonate precipitation as ikaite in the FF and throughout
448 the ice. Precipitation of ikaite in sea ice is not yet fully understood. Ikaite precipitation seems
449 to be favored by near-freezing temperatures, alkaline conditions, elevated phosphate
450 concentrations and/or by the presence of certain additives like amino acids [*J L Bischoff et al.*,
451 1993a; *Whiticar and Suess*, 1998; *Buchardt et al.*, 2001; *Selleck et al.*, 2007]. Our results
452 suggest that all these conditions were satisfied at our sampling location. In addition, the role
453 of sea ice as a trigger for tropospheric ozone depletion as a consequence of low pH due to
454 $CaCO_3$ precipitation and related reduced sea ice buffer capacity should be considered with
455 caution. Investigations are needed to further understand and budget ikaite precipitation in sea
456 ice.

457 According to the amount of $CaCO_3$ precipitated in FF and in the upper layer of the ice (top 10
458 cm), the amount of CO_2 generated by this process is therefore minor compared to the total
459 flux estimated by DIC depletion. This decrease of 2069 µmol kg^{-1} melted sample mainly
460 corresponds to a release of CO_2 from the ice to the atmosphere due to expulsion of brine
461 supersaturated in CO_2. If the ice was between 2 days and 7 days old, the loss in DIC
462 corresponded to a CO_2 flux ranging from 20 mmol m^{-2} d^{-1} to 40 mmol m^{-2} d^{-1}.

463 The air-sea ice CO_2 fluxes derived from the DIC depletion are large compared to the overall
464 amount of DIC within the ice. If we compare the DIC deficit of the ice (2069 µmol kg^{-1}
465 melted sample) to the DIC concentration of the underlying seawater (2230 µmol kg^{-1}) about
466 92% of the DIC in the top 7.5 cm of the ice are rejected into the atmosphere. This is not
467 surprising since it is well documented that the ice rejects more than two third of its salt,
468 mainly to the underlying water. However, during our survey of the first stage of sea ice
469 growth, the formation of frost flowers indicated an upward rejection of brine at the air-ice
470 interface. While most of the salts remain at the surface of the ice, gases mix with the
471 atmosphere, and are therefore effectively removed from the ice. This explains why gases are
472 more efficiently expelled from the ice compared to salts in the case of upward brine expulsion
473 during the first stage of sea ice formation and is consistent with the observations of *Loose et*
474 *al.* [2009] who show enhanced rejection of gas (O_2) compared to salt. Brine expulsion appears
475 to support significant release of CO_2 from the top of polar ocean waters to the atmosphere
476 during the first stages of sea ice growth. This leads to a significant depletion in DIC of the top
477 centimeters of the ice.

478 # Acknowledgements

479 The authors warmly thank Pr. Hajo Eicken for his strong and crucial support to the project
480 and Pr. Perovich from Dartmouth University and the rest of the sea ice group of the

Geophysical Institute of the University of Alaska Fairbanks for setting the sea ice mass balance buoy and providing data. We are indebted to the Barrow Arctic Science Consortium and the North Slope Borough for their logistical support, to Dr. Giles Marion for his help in understanding FREZCHEM model. We thank Dr. Helmuth Thomas and three anonymous reviewers for their comments that enhanced the quality of the manuscript. This research was supported by the F.R.S-FNRS (contract 2.4584.09), with which BD is a research associate, the National Science Foundation, the University of Alaska Fairbanks and the Belgian Science Policy (contract SD/CA/03A). NXG received a PhD grant from the Fonds pour la Formation à la Recherche dans l'Industrie et l'Agriculture and now received financial support from the Canada Excellence Research Chair (CERC) program. G.N. and G.D. have been supported by the DFG by grant NE 1564/1-1 (SPP 1158). This is MARE contribution no. XXX.

References

Alvarez-Aviles, L., W. R. Simpson, T. A. Douglas, M. Sturm, D. Perovich, and F. Domine (2008), Frost flower chemical composition during growth and its implications for aerosol production and bromine activation, *J. Geophys. Res.-Atmos.*, *113*(D21).

Arrigo, K. R., and C. W. Sullivan (1992), The influence of salinity and temperature covariation on the photophysiological characteristics of Antarctic sea ice microalgae, *J. Phycol.*, *28*(6), 746-756.

Arrigo, K. R., T. Mock, and P. M. Lizotte (2010), Primary producers and sea ice, in *Sea Ice - second edition*, edited by Wiley-Blackwell, pp. pp. 283 - 326, Oxford.

Assur, A. (1958), Composition of sea ice and its tensile strength, in *Arctic Sea Ice*, edited by N. A. o. S.-N. R. Concil, Easton, Maryland.

Bates, N. R., and J. T. Mathis (2009), The Arctic Ocean marine carbon cycle: evaluation of air-sea CO_2 exchanges, ocean acidification impacts and potential feedbacks, *Biogeosciences*, *6*(11), 2433-2459.

Bischoff, J. L., J. A. Fitzpatrick, and R. J. Rosenbauer (1993a), The solubility and stabilization of ikaite ($CaCO_3.6H_2O$) from 0°C to 25°C environmental and paleoclimatic implications for Thinolite Tufa, *J. Geol.*, *101*(1), 21-33.

509 Bischoff, J. L., S. Stine, R. J. Rosenbauer, J. A. Fitzpatrick, and T. W. Stafford (1993b), Ikaite
510 precipitation by mixing of shoreline springs and lake water, Mono Lake, California, USA,
511 *Geochimica Et Cosmochimica Acta*, *57*(16), 3855-3865.

512 Bischoff, W. D., S. K. Sharma, and F. T. Mackenzie (1985), Carbonate ion disorder in
513 synthetic and biogenic magnesian calcites: a Raman spectral study, *American Mineralogist*,
514 *70*, 581-589.

515 Bowman, J. S., and J. W. Deming (2010), Elevated bacterial abundance and exopolymers in
516 saline frost flowers and implications for atmospheric chemistry and microbial dispersal,
517 *Geophysical Research Letters*, *37*(L13501).

518 Buchardt, B. (2004), Ikaite geochemistry and formation of submarine tufas in Greenland,
519 *Geochimica Et Cosmochimica Acta*, *68*(11), A348-A348.

520 Buchardt, B., C. Israelson, P. Seaman, and G. Stockmann (2001), Ikaite tufa towers in Ikka
521 Fjord, southwest Greenland: Their formation by mixing of seawater and alkaline spring water,
522 *Journal of Sedimentary Research*, *71*(1), 176-189.

523 Delille, B. (2006), Inorganic carbon dynamics and air-ice-sea CO_2 fluxes in the open and
524 coastal waters of the Southern Ocean, 296 pp, Université de Liège, Liège.

525 Delille, B., B. Jourdain, A. V. Borges, J. L. Tison, and D. Delille (2007), Biogas (CO_2, O-2,
526 dimethylsulfide) dynamics in spring Antarctic fast ice, *Limnology and Oceanography*, *52*(4),
527 1367-1379.

528 Deming, J. W. (2010), Sea ice bacteria and viruses, in *Sea Ice, second edition*, edited by D. N.
529 Thomas and G. S. Dieckmann, pp. 1-22, Wiley- Blackwell, Oxford.

530 Dickson, A. G., and F. J. Millero (1987), A comparison of the equilibrium constants for the
531 dissociation of carbonic acid in seawater media, *Deep Sea Research*, *I*(34), 1733-1743.

532 Dieckmann, G. S., G. Nehrke, C. Uhlig, J. Göttlicher, S. Gerland, M. A. Granskog, and D. N.
533 Thomas (2010), Brief communication: Ikaite ($CaCO_3.6H_2O$) discovered in Arctic sea ice, *The*
534 *Cryosphere*, *4*, 227-230.

535 Dieckmann, G. S., G. Nehrke, S. Papadimitriou, J. Gottlicher, R. Steininger, H. Kennedy, D.
536 Wolf-Gladrow, and D. N. Thomas (2008), Calcium carbonate as ikaite crystals in Antarctic
537 sea ice, *Geophysical Research Letters*, *35*(8).

538 DOE (Ed.) (1994), *Handbook of methods for the analysis of the various parameters of the*
539 *carbon dioxide system in sea water*.

540 Domine, F., A. S. Taillandier, and W. R. Simpson (2005), Specific surface area, density and
541 microstructure of frost flowers, *Geophysical Research Letters*, *32*(L13502).

Druckenmiller, M. L., H. Eicken, M. A. Johnson, D. J. Pringle, and C. C. Williams (2009), Toward an integrated coastal sea-ice observatory: System components and a case study at Barrow, Alaska, *Cold Regions Science and Technology*, *56*(2-3), 61-72.

Ehn, J. K., B. J. Hwang, R. Galley, and D. G. Barber (2007), Investigations of newly formed sea ice in the Cape Bathurst polynya: 1. Structural, physical, and optical properties, *Journal of Geophysical Research-Oceans*, *112*(C5).

Eicken, H. (2003), From the microscopic to the macroscopic to the regional scale, growth, microstrucutre and properties of sea ice, in *Sea Ice - An introduction to its physics, biology, chemistry and geology*, edited by B. Science, pp. pp. 22 - 81, London.

Frankignoulle, M. (1988), Field-Measurements of Air Sea CO_2 Exchange, *Limnology and Oceanography*, *33*(3), 313-322.

Frankignoulle, M., and A. V. Borges (2001), Direct and indirect pCO_2 measurements in a wide range of pCO_2 and salinity values (the Scheldt estuary), *Aquatic Geochemistry*, *7*(4), 267-273.

Geilfus, N. X., G. Carnat, T. N. Papakyriakou, J. L. Tison, B. Else, H. Thomas, E. H. Shadwick, and B. Delille (2012), pCO2 dynamics and related air-ice CO2 fluxes in the Arctic coastal zone (Amundsen Gulf, Beaufort Sea), *Journal of Geophysical Research*, *117*(COOG10).

Gleitz, M., M. R. v.d.Loeff, D. N. Thomas, G. S. Dieckmann, and F. J. Millero (1995), Comparison of summer and winter in organic carbon, oxygen and nutrient concentrations in Antarctic sea ice brine, *Mar. Chem.*, *51*(2), 81-91.

Golden, K. M., H. Eicken, A. L. Heaton, J. Miner, D. J. Pringle, and J. Zhu (2007), Thermal evolution of permeability and microstructure in sea ice, *Geophysical Research Letters*, *34*(16).

Gosselin, M., M. Levasseur, P. A. Wheeler, R. A. Horner, and B. C. Booth (1997), New measurements of phytoplankton and ice algal production in the Arctic Ocean, *Deep Sea Research II*, *44*(8), 1623 - 1644.

Gran, G. (1952), Determination of the equivalence point in potentiometric titration, *Analyst*, *Part II*(77), 661-671.

Grasshoff, K., M. Ehrhardt, and K. Kremling (1983), Methods of sea water analysis, *Verlag Chemie*.

Kennedy, G. L., D. M. Hopkins, and W. J. Pickthorn (1987), Ikaite, the glendonite precursor, in estuarine sediments at Barrow, Arctic Alaska, *Geological Survey of Alaska Annual Meeting*, *Abstract, Programme 9*, 725.

576 Krembs, C., H. Eicken, K. Junge, and J. W. Deming (2002), High concentrations of
577 exopolymeric substances in Arctic winter sea ice: implications for the polar ocean carbon
578 cycle and cryoprotection of diatoms, *Deep-Sea Research Part I-Oceanographic Research*
579 *Papers*, *49*(12), 2163-2181.

580 Lee, S. H., T. E. Whitledge, and S. H. Kang (2008), Spring time production of bottom ice
581 algae in the landfast sea ice zone at Barrow, Alaska, *Journal of Experimental Marine Biology*
582 *and Ecology*, *367*(2), 204-212.

583 Lepparanta, M. (1993), A review of analytical models of sea-ice growth, *Atmos.-Ocean*,
584 *31*(1), 123-138.

585 Loose, B., W. R. McGillis, P. Schlosser, D. Perovich, and T. Takahashi (2009), Effects of
586 freezing, growth, and ice cover on gas transport processes in laboratory seawater experiments,
587 *Geophysical Research Letters*, *36*(5), L05603.

588 Marion, G. M. (2001), Carbonate mineral solubility at low temperatures in the Na-K-Mg-Ca-
589 H-Cl-SO_4-OH-HCO_3-CO_3-CO_2-H_2O system, *Geochimica Et Cosmochimica Acta*, *65*(12),
590 1883-1896.

591 Mathis, J. T., N. R. Bates, D. A. Hansell, and T. Babila (2009), Net community production in
592 the northeastern Chukchi Sea, *Deep-Sea Research Part Ii-Topical Studies in Oceanography*,
593 *56*(17), 1213-1222.

594 Mehrbach, C., C. H. Culberson, J. E. Hawley, and R. M. Pytkowicz (1973), Measurements of
595 the apparent dissociation constants of carbonic acid in seawater at atmospheric pressure,
596 *Limnology and Oceanography*, *18*, 897-907.

597 Miller, L., T. Papakyriakou, R. E. Collins, J. Deming, J. Ehn, R. W. Macdonald, A. Mucci, O.
598 Owens, M. Raudsepp, and N. Sutherland (2011), Carbon Dynamics in Sea Ice: A Winter Flux
599 Time Series, *Journal of Geophysical Research-Oceans*, *116*(C02028).

600 Morin, S., G. M. Marion, R. von Glasow, D. Voisin, J. Bouchez, and J. Savarino (2008),
601 Precipitation of salts in freezing seawater and ozone depletion events: a status report, *Atmos.*
602 *Chem. Phys.*, *8*(23), 7317-7324.

603 Munro, D. R., R. B. Dunbar, D. A. Mucciarone, K. R. Arrigo, and M. C. Long (2010), Stable
604 isotope composition of dissolved inorganic carbon and particulate organic carbon in sea ice
605 from the Ross Sea, Antarctica, *Journal of Geophysical Research-Oceans*, *115*.

606 Nomura, D., H. Yoshikawa-Inoue, and T. Toyota (2006), The effect of sea-ice growth on air-
607 sea CO_2 flux in a tank experiment, *Tellus Series B-Chemical and Physical Meteorology*,
608 *58*(5), 418-426.

609 Nomura, D., H. Yoshikawa-Inoue, T. Toyota, and K. Shirasawa (2010a), Effects of snow,
610 snow-melting and re-freezing processes on air-sea ice CO_2 flux, *Journal of Glaciology*.

611 Nomura, D., H. Eicken, R. Gradinger, and K. Shirasawa (2010b), Rapid physically driven
612 inversion of the air-sea ice CO_2 flux in the seasonal landfast ice off Barrow, Alaska after onset
613 surface melt, *Continental Shelf Research*, *30*(19), 1998-2004.

614 Papadimitriou, S., H. Kennedy, G. Kattner, G. S. Dieckmann, and D. N. Thomas (2004),
615 Experimental evidence for carbonate precipitation and CO_2 degassing during sea ice
616 formation, *Geochimica et Cosmochimica Acta*, *68*(8), 1749-1761.

617 Papadimitriou, S., D. N. Thomas, H. Kennedy, C. Haas, H. Kuosa, A. Krell, and G. S.
618 Dieckmann (2007), Biogeochemical composition of natural sea ice brines from the Weddell
619 Sea during early austral summer, *Limnology and Oceanography*, *52*(5), 1809-1823.

620 Papakyriakou, T., and L. Miller (2011), Springtime CO_2 exchange over seasonal sea ice in the
621 Canadian Arctic Archipelago, *Annals of Glaciology*, *52*(57).

622 Perovich, D. K., and J. A. Richter-Menge (1994), Surface characteristics of lead ice, *Journal*
623 *of Geophysical Research-Oceans*, *99*(C8), 16341-16350.

624 Piot, M., and R. von Glasow (2008), The potential importance of frost flowers, recycling on
625 snow, and open leads for ozone depletion events, *Atmos. Chem. Phys.*, *8*(9), 2437-2467.

626 Rankin, A. M., V. Auld, and E. W. Wolff (2000), Frost flowers as a source of fractionated sea
627 salt aerosol in the polar regions, *Geophysical Research Letters*, *27*(21), 3469-3472.

628 Rankin, A. M., E. W. Wolff, and S. Martin (2002), Frost flowers: Implications for
629 tropospheric chemistry and ice core interpretation, *J. Geophys. Res.-Atmos.*, *107*(D23).

630 Rysgaard, S., R. N. Glud, M. K. Sejr, J. Bendtsen, and P. B. Christensen (2007), Inorganic
631 carbon transport during sea ice growth and decay: A carbon pump in polar seas, *Journal of*
632 *Geophysical Research-Oceans*, *112*(C3).

633 Rysgaard, S., J. Bendtsen, L. T. Pedersen, H. Ramlov, and R. N. Glud (2009), Increased CO_2
634 uptake due to sea ice growth and decay in the Nordic Seas, *Journal of Geophysical Research*,
635 *114*(C09011).

636 Sander, R., J. Burrows, and L. Kaleschke (2006), Carbonate precipitation in brine - a potential
637 trigger for tropospheric ozone depletion events, *Atmos. Chem. Phys.*, *6*, 4653-4658.

638 Selleck, B. W., P. F. Carr, and B. G. Jones (2007), A Review and Synthesis of Glendonites
639 (Pseudomorphs after Ikaite) with New Data: Assessing Applicability as Recorders of Ancient
640 Coldwater Conditions, *Journal of Sedimentary Research*, *77*(11), 980-991.

641 Semiletov, I. P., A. Makshtas, S. I. Akasofu, and E. L. Andreas (2004), Atmospheric CO_2
642 balance: The role of Arctic sea ice, *Geophysical Research Letters*, *31*(5).

643 Semiletov, I. P., I. Pipko, I. Repina, and N. E. Shakhova (2007), Carbonate chemistry
644 dynamics and carbon dioxide fluxes across the atmosphere-ice-water interfaces in the Arctic
645 Ocean: Pacific sector of the Arctic, *Journal of Marine Systems*, *66*(1-4), 204-226.

646 Takahashi, T., et al. (2009), Climatological mean and decadal change in surface ocean pCO_2,
647 and net sea-air CO_2 flux over the global oceans, *Deep-Sea Research Part Ii-Topical Studies in*
648 *Oceanography*, *56*(8-10), 554-577.

649 Thomas, D. N., S. Papadimitriou, and C. Michel (2010), Biogeochemistry of sea ice, in *Sea*
650 *Ice - second edition*, edited by B. Science, p. 621, London.

651 Timco, G. W., and R. M. W. Frederking (1996), A review of sea ice density, *Cold Regions*
652 *Science and Technology*, *24*(1), 1-6.

653 Tison, J. L., A. Worby, B. Delille, F. Brabant, S. Papadimitriou, D. Thomas, J. de Jong, D.
654 Lannuzel, and C. Haas (2008), Temporal evolution of decaying summer first-year sea ice in
655 the Western Weddell Sea, Antarctica, *Deep-Sea Research Part Ii-Topical Studies in*
656 *Oceanography*, *55*(8-9), 975-987.

657 Weeks, W. F., and S. F. Ackley (1982), *The growth, structure, and properties of sea ice.*, 117
658 pp., CRREL Monograph.

659 Whiticar, M. J., and E. Suess (1998), The cold carbonate connection between Mono Lake,
660 California and the Bransfield Strait, Antarctica, *Aquatic Geochemistry*, *4*(3-4), 429-454.

661 Zemmelink, H. J., B. Delille, J. L. Tison, E. J. Hintsa, L. Houghton, and J. W. H. Dacey
662 (2006), CO_2 deposition over the multi-year ice of the western Weddell Sea, *Geophysical*
663 *Research Letters*, *33*(13).

664

665

666

667 Figure captions

668 Figure 1: Location of the sampling area (black star) at Barrow, Alaska, and pictures of the
669 sampling site. The chamber of accumulation is 20cm of diameter

670 Figure 2: Pictures of ikaite crystals. From *Dieckmann et al.* [2008] (**A**) and from our melted
671 sea ice, direct measurement under a binocular microscope (**B**) and from a Raman (**C**).

672 Figure 3: Temperature and salinity and brine volume profile at the Barrow young ice site

673 Figure 4: Textural features of the young sea ice include: frost flowers (**FF**), brine skim (**BS**),
674 fine-grained granular ice (**FG**), orbicular granular ice (**G**), intermediate granular/columnar ice
675 (**G/C**) and columnar ice (**C**).
676 The black and white scale represents a centimetre scale.

677 Figure 5: Profiles of pH (a), TA_f and DIC_f (b), DIC_{10} (c), difference between the DIC_{th} and
678 DIC_f (d), ratio between TA_b and DIC_b (e) and the difference between bulk and filtrated TA
679 with the estimation of the precipitated amount of calcium carbonate (f).

680 Figure 6: Successive X-ray diffraction patterns of crystals stored on Millipore filters at -25°C
681 (**a**., **b**., **c**.), X-ray diffraction from same sample after 1 day at room temperature (**d**.). Line
682 patterns for **e.** Halite, **d.** Calcite from the RRUFF data base. The data base numbers are
683 R070534 for Halite and R040070 for Calcite.

684 Figure 7: Raman spectra of calcite standard (blue), ikaite (red) and sample (green).

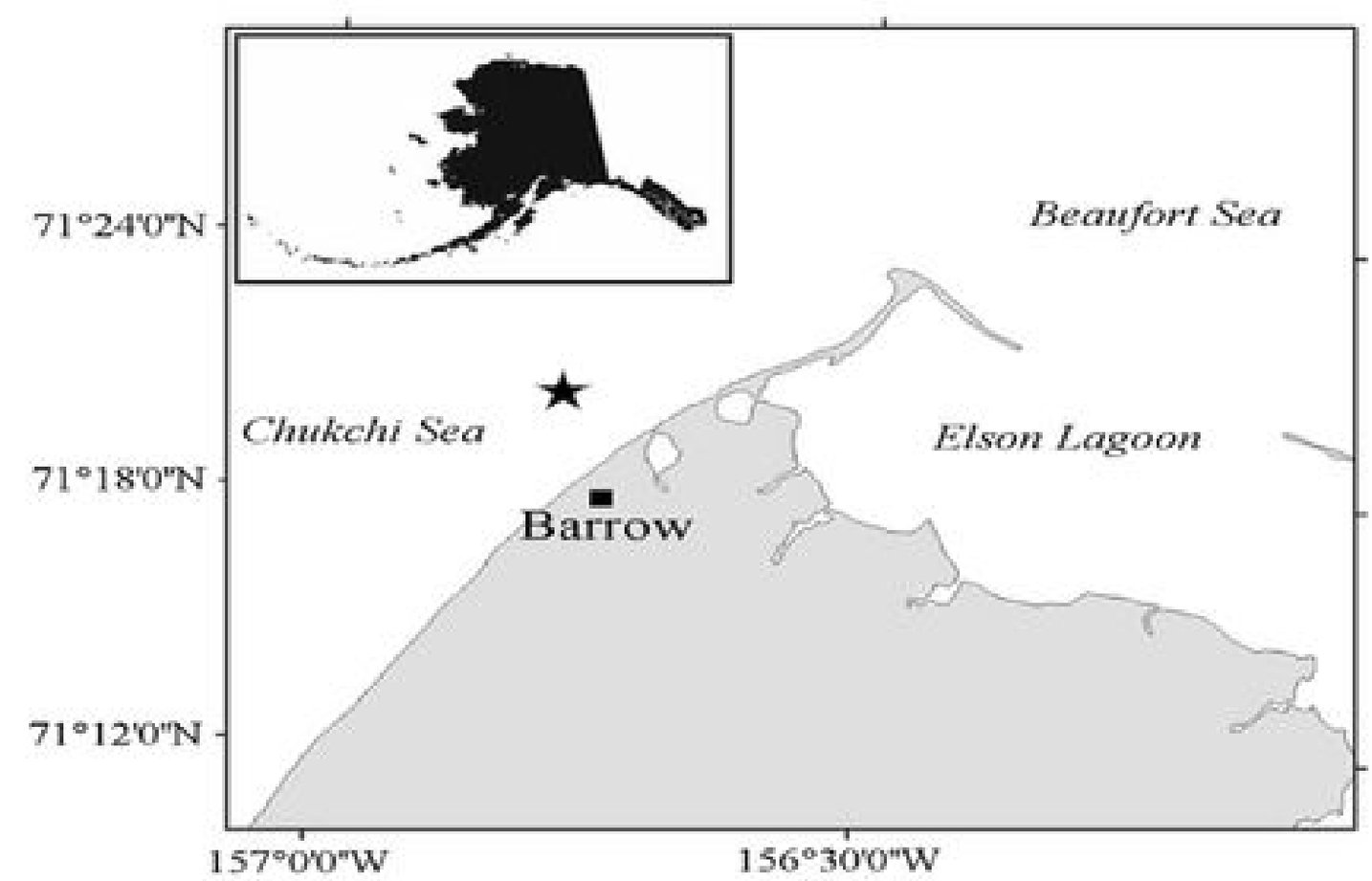
71°24'0"N
71°18'0"N
71°12'0"N
157°0'0"W
156°30'0"W
Beaufort Sea
Chukchi Sea
Elson Lagoon
Barrow

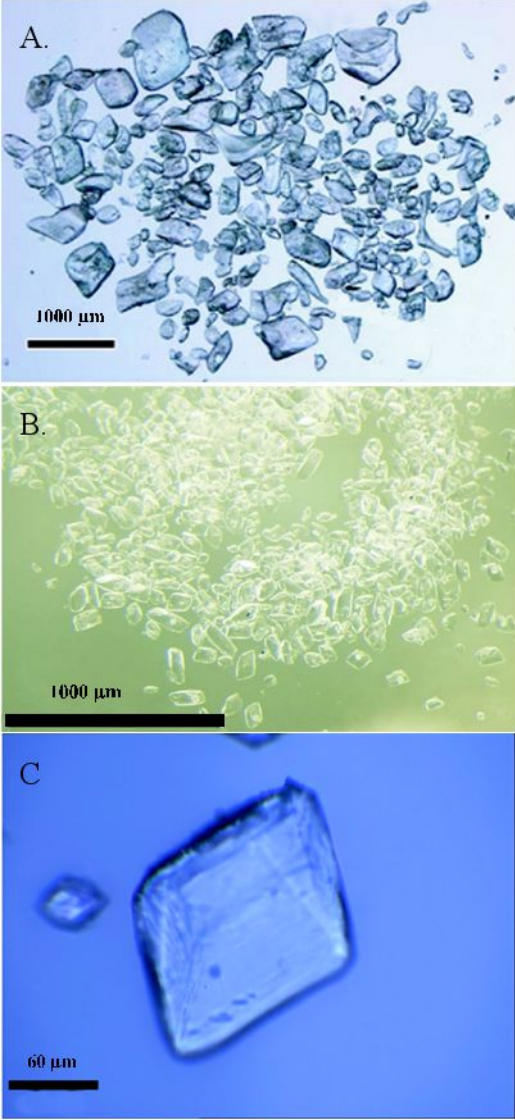
A.
1000 µm
B.
1000 µm
C
60 µm

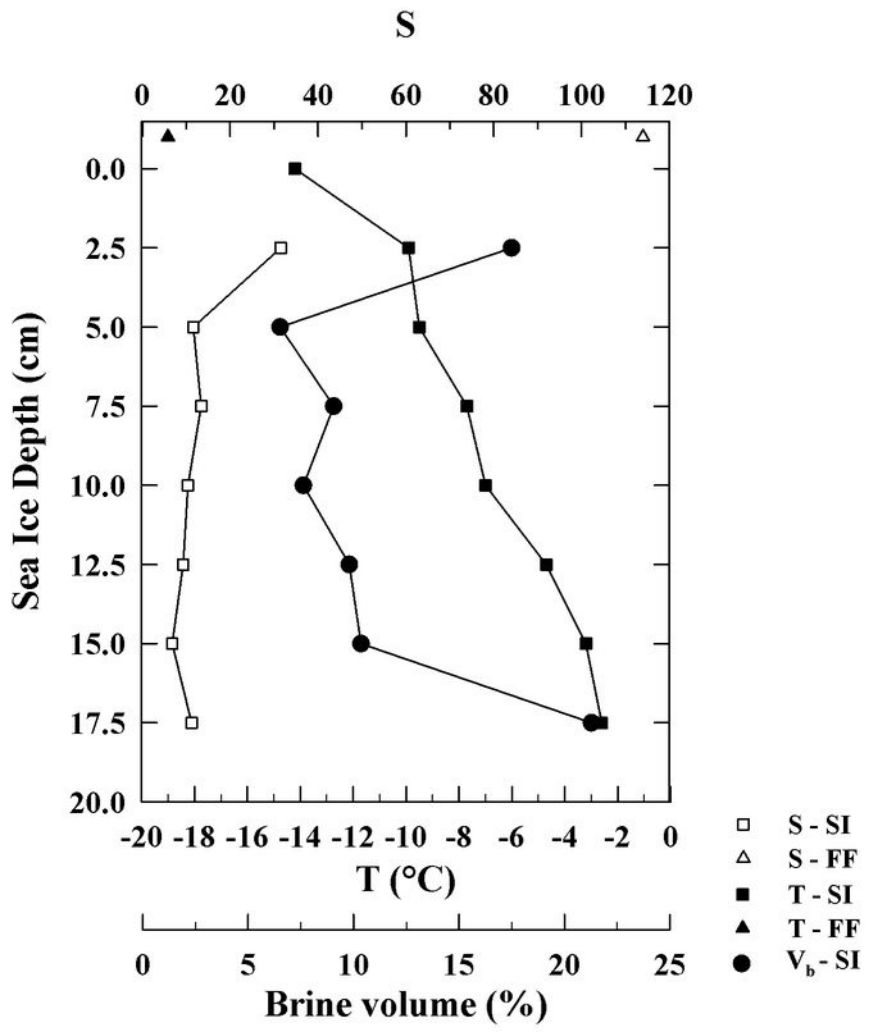
S
0
20
40
60
80
100
120
Sea Ice Depth (cm)
0.0
2.5
5.0
7.5
10.0
12.5
15.0
17.5
20.0
-20
-18
-16
-14
-12
-10
-8
-6
-4
-2
0
T (°C)
0
5
10
15
20
25
Brine volume (%)
S - SI
S - FF
T - SI
T - FF
V_b - SI

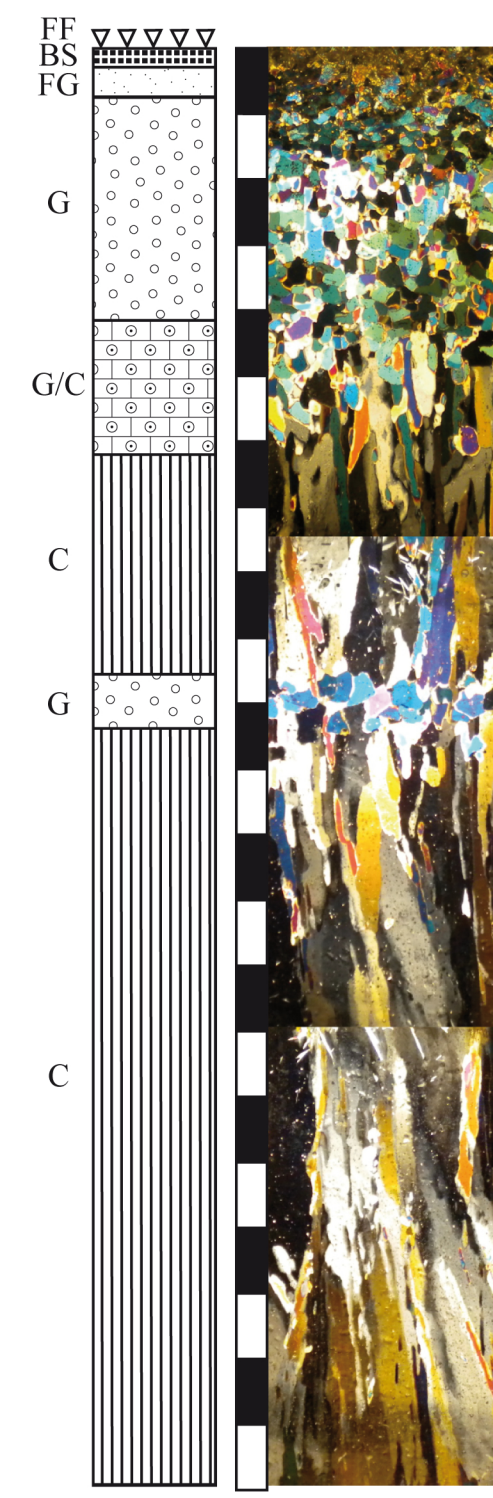
FF
BS
FG
G
G/C
C
G
C

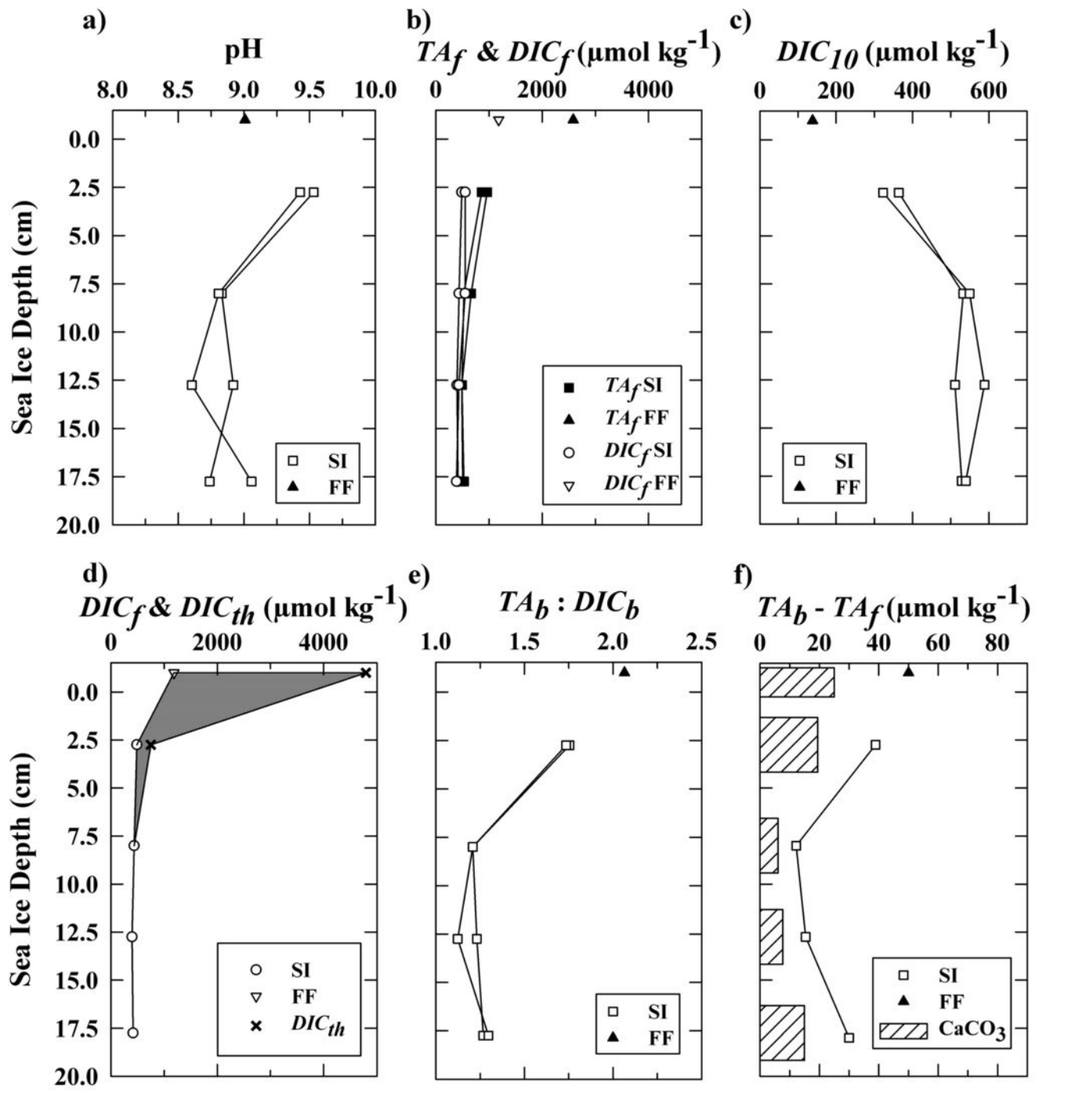
a)
pH
8.0
8.5
9.0
9.5
10.0
b)
TA_f & DIC_f (µmol kg^{-1})
0
2000
4000
c)
DIC_{10} (µmol kg^{-1})
0
200
400
600
Sea Ice Depth (cm)
0.0
2.5
5.0
7.5
10.0
12.5
15.0
17.5
20.0
SI
FF
TA_f SI
TA_f FF
DIC_f SI
DIC_f FF
d)
DIC_f & DIC_{th} (µmol kg^{-1})
0
2000
4000
DIC_{th}
e)
TA_b : DIC_b
1.0
1.5
2.0
2.5
f)
TA_b - TA_f (µmol kg^{-1})
0
20
40
60
80
$CaCO_3$

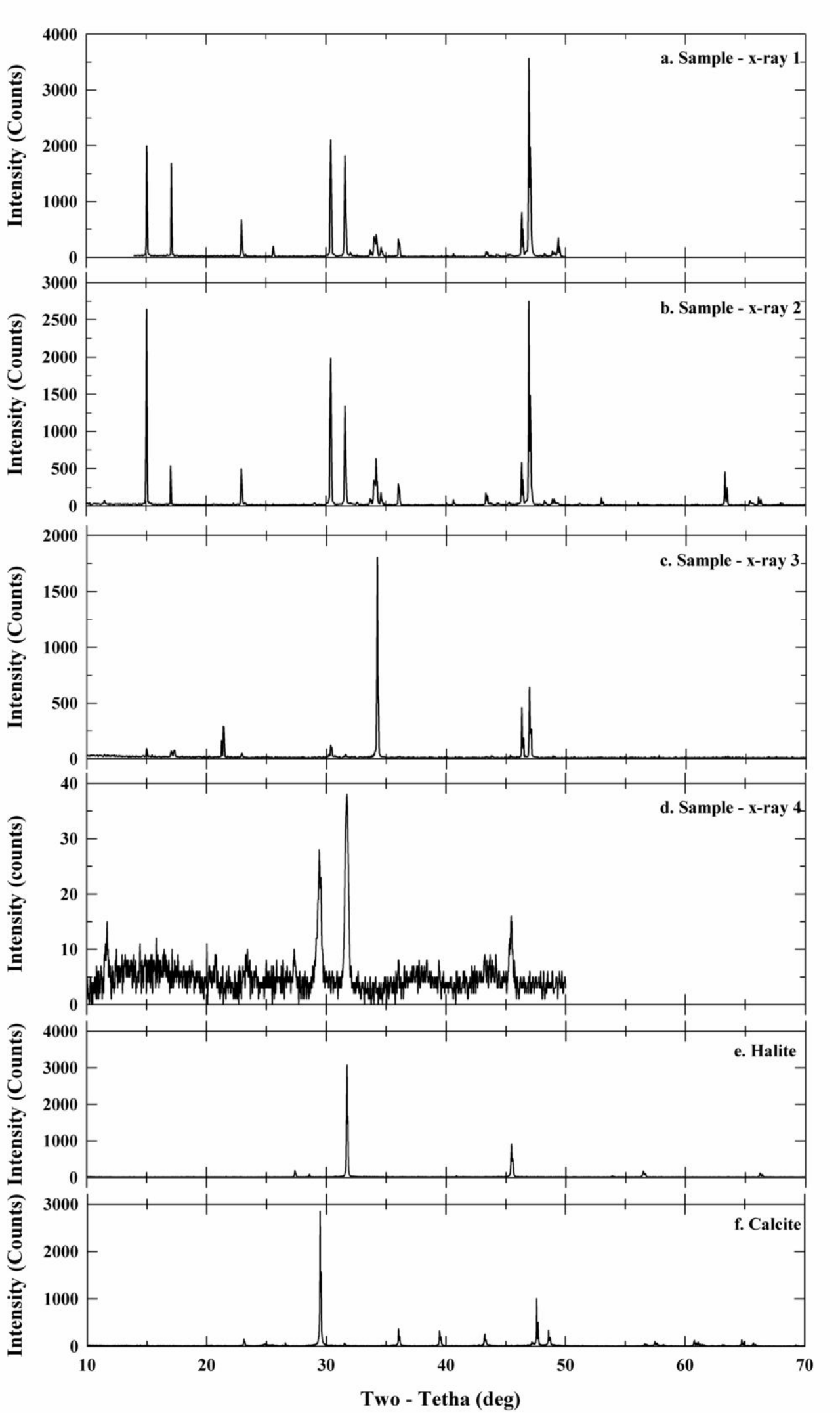
a. Sample - x-ray 1
b. Sample - x-ray 2
c. Sample - x-ray 3
d. Sample - x-ray 4
e. Halite
f. Calcite
Intensity (Counts)
Intensity (counts)
Two - Tetha (deg)

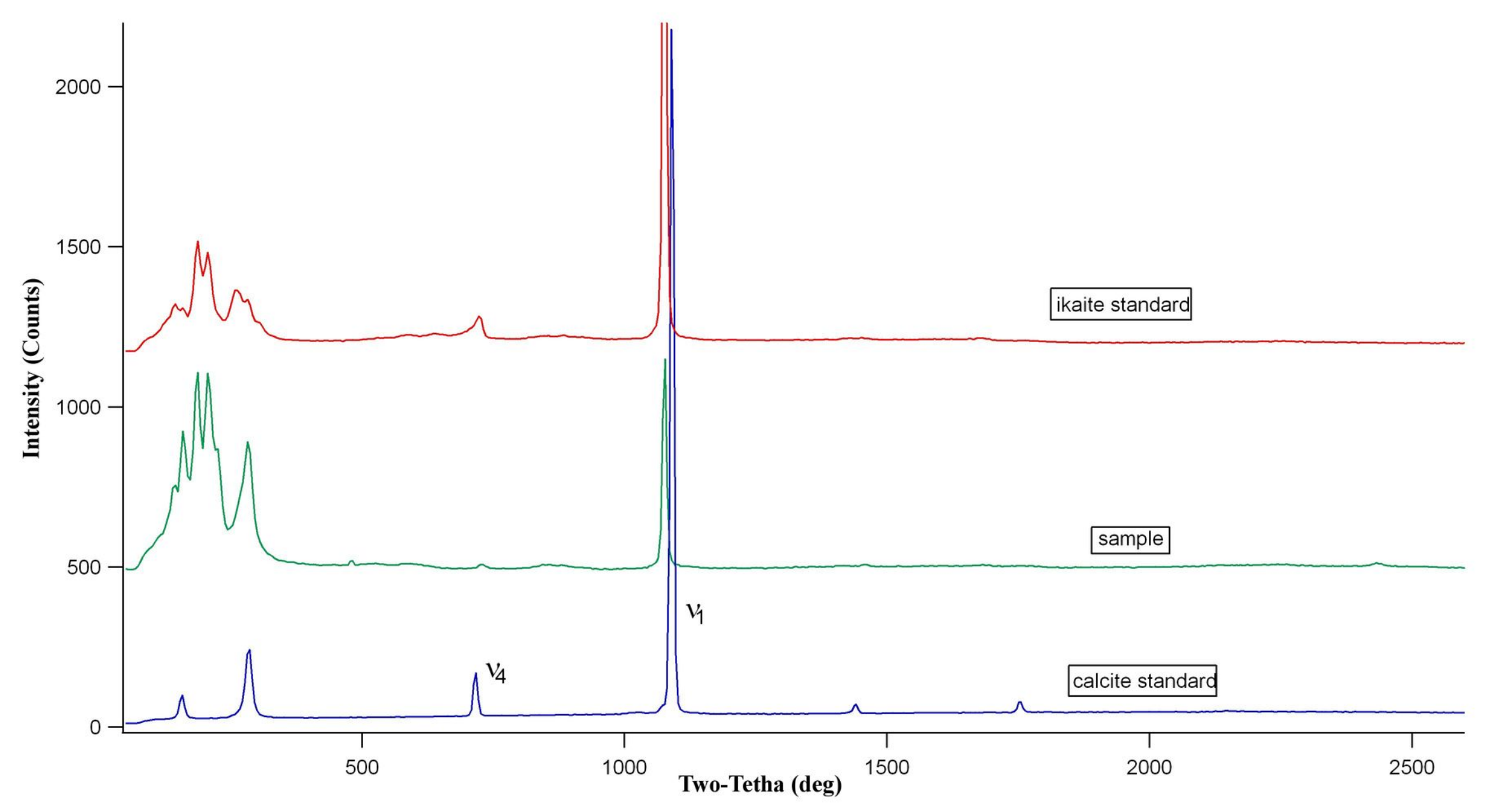
Intensity (Counts)
2000
1500
1000
500
0
ikaite standard
sample
calcite standard
ν_1
ν_4
500
1000
1500
2000
2500
Two-Tetha (deg)